

Grain-Boundary Topological Phase Transitions

Kongtao Chen^a, David J. Srolovitz^b, and Jian Han^{b,1}

^aDepartment of Materials Science and Engineering, University of Pennsylvania, Philadelphia, PA 19104 USA; ^bDepartment of Materials Science and Engineering, City University of Hong Kong, Kowloon, Hong Kong SAR, China

The formation and migration of disconnections (line defects constrained to the grain boundary (GB) plane with both dislocation and step character) control many of the kinetic and dynamical properties of GBs and the polycrystalline materials of which they are central constituents. We demonstrate that GBs undergo a finite-temperature topological phase transition of the Kosterlitz-Thouless (KT) type. This phase transition corresponds to the screening of long-range interactions between (and unbinding of) disconnections. This phase transition leads to abrupt change in the behavior of GB migration, GB sliding, and roughening. We analyze this KT transition through mean-field theory, renormalization group theory, and kinetic Monte Carlo simulations, and examine how this transition affects microstructure-scale phenomena such as grain growth stagnation, abnormal grain growth and superplasticity.

materials science | thermodynamics | phase transition | grain boundary
| grain growth

Physical properties of polycrystalline materials depend strongly on the properties of their constituent grain boundaries (GBs). Like most material properties, GB properties are functions of temperature and may change abruptly at temperatures corresponding to phase transitions. Such GB phase transitions may explain the existence of critical temperatures at which abrupt changes in the nature of several physical phenomena, including grain growth stagnation (1) and superplasticity (2).

There are several types of GB phase transitions discussed in the literature. These include thermodynamic phase transitions such as GB structural transitions or faceting/defaceting transitions (which are first-order) (3–5), roughening transitions (divergence in the height-height correlation function) which may be continuous (6), and improper transitions where the GB transforms from solid-like to glass-like (7). In this paper, we discuss a new class of fundamentally different GB phase transitions. We identify a GB topological phase transition of a type of the class originally discussed by Kosterlitz and Thouless (8). Such topological transitions may be thought of as defect binding/unbinding transitions. The most important type of defects for GB dynamics are disconnections (9). Disconnections are line defects, constrained to lie within the GB and characterized by both Burgers vector \mathbf{b} and step height h . The set of possible disconnection modes $\{\mathbf{b}, h\}$ is set by GB bicrystallography. Disconnections (like dislocations) are topological defects, as seen through a Burgers circuit analysis (9).

Below the topological or Kosterlitz-Thouless (KT) transition temperature T_{KT} , the interaction between disconnections is long-range, decaying as the inverse of their separation. The formation and migration of disconnections are severely restricted and GB mobility tends to be small (with important exceptions). On the other hand, above T_{KT} , the long-range elastic field of disconnections is effectively screened. Hence, the KT transition may be viewed as a screening (or sliding)

transition, where the screening parameter (dielelectric constant) diverges at T_{KT} . The KT transition leads to abrupt changes in the GB migration mobility, roughness, sliding coefficient, etc.

While the KT transition leads to GB roughening, this transition fundamentally differs from the roughening transition widely discussed in the literature (6). While this classic roughening phase transition is topological, the steps have no long-range elastic interactions and are not topological defects (nonlocal imperfections corresponding to singularities in an order parameter characterizing a broken symmetry (10)). On the other hand, the dislocation nature of disconnections implies that disconnections are fundamentally topological defects. Hence, the KT transition discussed in this paper corresponds to the screening of long-range elastic interactions, while the classical roughening transition arises from topologically stable configurations of steps (without long-range interactions).

We analyze the KT transition first through mean-field theory, then apply renormalization group analysis to accurately predict the main features of this transition by formal extension to the thermodynamic limit (i.e., infinite length scales). The results are confirmed through a series of kinetic Monte Carlo (kMC) simulations. Our analysis shows that the Kosterlitz-Thouless (KT) transition temperature depends on the driving force for GB motion. For example, in curvature-driven grain growth, we find that at a fixed temperature, large grains are more likely to be below T_{KT} (low mobility) and small grains above it (high mobility). This is a possible explanation of why grain growth in pure materials often stagnates at large grain size and superplasticity is generally restricted to small grain sizes and high temperatures. We confirm these results by comparing our renormalization group prediction of the grain size at which grain growth stagnation occurs with simulation data from the literature (1).

Significance Statement

We reveal the existence of a topological phase transition (Kosterlitz-Thouless type) in grain boundaries (GBs) – important internal surfaces in crystalline materials. GB dynamics are controlled by the formation/migration of line defects (disconnections) with dislocation and step character. Below the GB KT transition, disconnections of opposite signs are bound as pairs, while above it, they unbind and proliferate. We demonstrate that GB KT transitions provide a fundamental understanding of many GB properties, the temporal evolution of microstructure and how it deforms/degrades under stress.

All authors designed the research and wrote the paper; K.C. performed simulations and analyzed data.

The authors declare no conflict of interest.

¹To whom correspondence should be addressed. E-mail: jianhan@cityu.edu.hk

Disconnection Topological Transitions

We describe the migration of GBs in terms of the motion of disconnections. Motion of disconnections leads to both GB migration (step motion) and shear across the GB (dislocation motion). We demonstrate that an abrupt change in GB behavior may result from an abrupt change in how disconnections interact; this is a topological phase transition.

We first consider the case of a dislocation in a two-dimensional (2d) elastic medium (x - y plane) interacting with dislocation dipoles, following the general approach originally described by Kosterlitz and Thouless (8). Here, we assume that the Burgers vectors are parallel to the x -axis: $\mathbf{b} = b\hat{\mathbf{x}}$. The elastic interaction energy of a test dislocation and another dislocation varies as the logarithm of their separation and the interaction force is minus the gradient of this energy with respect to test dislocation displacement (i.e., decaying as the inverse of their separation). When multiple dislocations are present, the total force on the test dislocation is simply the sum of the forces from each of these. The divergence of the force on the test dislocation (of unit \mathbf{b}) at \mathbf{r} , $\mathbf{f}(\mathbf{r})$ is proportional to the Burgers vector distribution around the test dislocation $\rho(\mathbf{r})$: $\nabla \cdot \langle \mathbf{f} \rangle = 4\pi K \rho(\mathbf{r})$, where $\rho(\mathbf{r})$ is the Burgers vector density and the constant $K \equiv \mu/[4\pi(1-\nu)]$ (μ and ν are the elastic shear modulus and Poisson ratio). (Angular brackets $\langle \dots \rangle$ denote the time average of a fluctuating quantity.) Dislocation dipoles in the material polarize (dislocations in the dipole separate) under the action of a (Peach-Koehler) force (11). The (polarized) dipole moment is $\int \langle \mathbf{p} \rangle d\mathbf{r} = \int \mathbf{r} \rho(\mathbf{r}) d\mathbf{r}$, where \mathbf{p} is the instantaneous dipole moment density. The distribution of polarized dipoles exert a force on the test dislocation: $\langle \mathbf{f}_p \rangle = -4\pi K \langle \mathbf{p} \rangle$. The total force on the test dislocation is the sum of the applied force \mathbf{f} and that associated with the induced dipoles: $\langle \mathbf{f}_t \rangle = \mathbf{f} + \langle \mathbf{f}_p \rangle = \mathbf{f} - 4\pi K \langle \mathbf{p} \rangle$. The dipole moment is induced by the total force, $\langle \mathbf{p} \rangle = \chi \langle \mathbf{f}_t \rangle$ (to leading order in the force), where, in analogy to electrostatics, we define the susceptibility (tensor) as $\chi \equiv (\partial \langle \mathbf{p} \rangle / \partial \langle \mathbf{f}_t \rangle)|_{\langle \mathbf{f}_t \rangle = 0}$.

The total force on the test dislocation can then be expressed as the external force *screened* by the induced dipoles $\langle \mathbf{f}_t \rangle = \mathbf{f}/\epsilon$, where ϵ is the diaelastic constant (akin to the dielectric constant in electrostatics). The diaelastic constant describes the strength of the screening of the applied force by the induced dislocation dipoles: $\epsilon \mathbf{I} = \mathbf{I} + 4\pi K \chi$ (\mathbf{I} is the identity matrix).

Disconnections on Grain Boundaries. We now apply this approach to disconnections on a nominally flat GB which, in this 2d model, is the line $y = 0$. In this case, the Burgers vector density is $\rho(x, y) = \rho(x)/\delta$, where δ is the disconnection core size. The external applied force on the test dislocation (with unit \mathbf{b}) is equal to the applied (shear) stress τ parallel to \mathbf{b} , $f = \tau$. In this case, $\epsilon = 1 + 4\pi K \chi$, where χ is the the xx component of the susceptibility tensor. The distribution of the dislocation dipole moment associated with all dipoles with separation smaller than r is $\langle p(r, x) \rangle = \int_{\delta}^r \langle br' \rangle n(r', x) dr'$, where $\langle br' \rangle$ is the moment of a dipole of separation r' and $n(r')$ is the number of dipoles with separation in $[r', r' + dr']$ per unit length between x and $x + dx$. Since we assume that the GB is uniform, we can drop the explicit dependence on x and write the susceptibility as $\chi(r) = (\partial \langle p \rangle / \partial f)|_{f=0} = \int_{\delta}^r \alpha(r') n(r') dr'$ ($\alpha(r') \equiv (\partial \langle br' \rangle / \partial \tau)|_{\tau=0}$ is the dipole polarizability). The

diaelastic constant, then, becomes

$$\epsilon(r) = 1 + 4\pi K \int_{\delta}^r \alpha(r') n(r') dr'. \quad [1]$$

We evaluate the dipole polarizability and dipole number density $n(r)$ by assuming that the dipoles are in thermal equilibrium (Maxwell-Boltzmann distribution) as in the Debye-Hückel approximation for charged fluids. The polarizability is

$$\alpha(r) = \frac{\partial}{\partial \tau} \frac{\sum_{b'=\pm b} b' r e^{-\beta(E_c - \tau b' r)}}{\sum_{b'=\pm b} e^{-\beta(E_c - \tau b' r)}} \bigg|_{\tau=0} = \beta b^2 r^2, \quad [2]$$

where E_c is the disconnection core energy (per unit length), w is the width of the system in the direction parallel to the disconnection line and $\beta \equiv w/k_B T$. The number density of dipoles of separation $[r, r + dr]$ is

$$n(r) = \delta^{-3} e^{-\beta[2E_c + V(r) - (\psi h + \tau b)r]}, \quad [3]$$

where ψ is the chemical potential jump across the GB (12), and the elastic interaction energy (per unit length) of the two disconnections in a dipole (separation r) is

$$V(r) = 2Kb^2 \int_{\delta}^r \frac{dr'}{r'(r')}. \quad [4]$$

This completes the derivation except for the determination of the dialectic constant $\epsilon(r)$, which can be determined through the self-consistent solution of Eq. (1) - Eq. (4). It is useful to define the following dimensionless (reduced) quantities: the reduced length $l \equiv \ln(r/\delta)$, the reduced inverse diaelastic constant $g \equiv \beta K b^2 / \epsilon(r)$, and the reduced dipole density $f \equiv \sqrt{r^3 n(r)}$. These substitutions reduce four coupled equations to just two:

$$\begin{cases} \frac{dg^{-1}}{dl} = 4\pi f^2 \\ \frac{d \ln f}{dl} = \frac{3}{2} - g + \frac{1}{2} \beta (\psi h + \tau b) r \end{cases}. \quad [5]$$

In the limit that $r \rightarrow \delta$ (i.e., $l = 0$), we find that $g(0) = \beta K b^2$ and $\ln f(0) = \beta[(\psi h + \tau b)\delta - 2E_c]/2$.

Topological Phase Transition. Here, we examine the topological phase transition that occurs for disconnections on a GB that is associated with the screening of the disconnection fields. We do this first via a simple mean-field analysis (designed to provide qualitative, physical understanding) and then via a more rigorous renormalization group approach.

As above, consider a bicrystal in 2d containing a flat 1d GB, as depicted in Fig. 1; the tilt axis is in z and the nominal GB normal is in y . We focus on a thermally equilibrated GB; incorporating the formation and annihilation of disconnection dipoles (Fig. 1a). The separation between the two disconnections in a dipole is r , the average distance between disconnection dipoles is L , and the size (length) of the GB is S . Since this model does not describe GB structure on the atomic-scale, it does not account for such phenomena as premelting.

For simplicity, we assume that there is only one type of disconnection dipole on the GB, i.e., disconnection mode $(\pm b, \pm h)$. If $b = 0$ (pure-step mode), the free energy change associated with disconnection dipole formation on a flat GB is

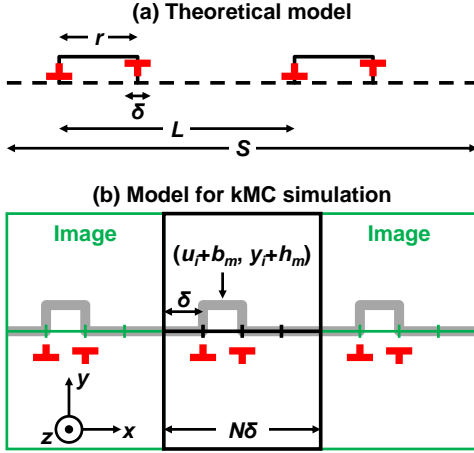


Fig. 1. (a) Disconnection dipoles on a 1d GB in 2d. δ , r , L and S denote the disconnection core size, the separation of the disconnections in a disconnection dipole, the average distance between the disconnection dipoles and the system size in the x -direction, respectively. (b) The states of the system at i before and after disconnection dipole nucleation are (u_i, y_i) and $(u_i + b_m, y_i + h_m)$, respectively, for a pair of disconnections of mode m at location i .

$F = 2E_c - k_B T \ln(S/\delta) < 0$ as $S \rightarrow \infty$, since the disconnection core energy E_c is independent of GB size S (9, 13, 14) and the configurational entropy is proportional to $\ln(S/\delta)$. This suggests that an infinitely large, 1d GB is rough at all $T > 0$ K (i.e., the roughening transition temperature is 0 K). If the GB is of finite size or where the GB is 2d, the roughening temperature is finite (15). If $b \neq 0$, however, both entropy and disconnection elastic energy are proportional to $\ln(S/\delta)$; this suggests that there will be a critical temperature above which the entropy term dominates the free energy such that the roughening transition temperature is finite (in all dimensions).

The effect of non-zero b can be understood as follows. At low T , disconnections exist as closely bound dipoles; while at high T the ratio of the separation between disconnections in a dipole to the spacing between dipoles is no longer small, such that the disconnection dipoles mix or, alternatively, the dipoles are unbound. Based on this idea, we can distinguish the low- T from high- T regimes based on whether $\langle r^2/L^2 \rangle \ll 1$ or $\gg 1$, respectively.

The energy of a disconnection dipole has the form $U(r) = 2E_c + V(r)$, where the elastic potential energy is $V(r) = 2Kb^2 \ln(r/\delta)$. We first assume that the equilibrium disconnection dipole density $1/L$ is low; i.e., $E_c \gg k_B T$. The ensemble average (square of the) disconnection separation in dipoles is

$$\langle r^2 \rangle = \frac{\int_{\delta}^{\infty} r^2 e^{-\beta U(r)} dr}{\int_{\delta}^{\infty} e^{-\beta U(r)} dr} = \delta^2 \left(\frac{2\beta K b^2 - 1}{2\beta K b^2 - 3} \right). \quad [6]$$

The average number of dipoles in length L can be obtained by the grand-canonical ensemble average:

$$\langle \mathcal{N} \rangle = \frac{\sum_{\mathcal{N}=0}^{\infty} \mathcal{N} \mathcal{Z}^{\mathcal{N}} \mathcal{P}^{\mathcal{N}}}{\sum_{\mathcal{N}=0}^{\infty} \mathcal{Z}^{\mathcal{N}} \mathcal{P}^{\mathcal{N}}} = \mathcal{Z} \mathcal{P} + \mathcal{O}(\mathcal{Z}^2),$$

where $\mathcal{Z} \equiv e^{-2\beta E_c}$ and

$$\mathcal{P} \equiv \frac{1}{\delta^2} \int_0^L dx \int_{\delta}^{\infty} e^{-\beta V(r)} dr = \frac{L/\delta}{2\beta K b^2 - 1}.$$

The average disconnection dipole density $\langle 1/L \rangle$ is obtained by setting $\langle \mathcal{N} \rangle = 1$:

$$\left\langle \frac{1}{L} \right\rangle = \left(\frac{1}{\delta} \right) \frac{e^{-2\beta E_c}}{2\beta K b^2 - 1}. \quad [7]$$

From Eq. (6) and Eq. (7), we find

$$\left\langle \frac{r^2}{L^2} \right\rangle = \frac{e^{-4\beta E_c}}{(2\beta K b^2 - 3)(2\beta K b^2 - 1)}. \quad [8]$$

This demonstrates that a critical temperature T_{KT} for which $\langle r^2/L^2 \rangle \rightarrow \infty$:

$$T_{KT} = 2Kb^2 w / 3k_B. \quad [9]$$

T_{KT} is the Kosterlitz-Thouless transition temperature. For $T < T_{KT}$, the disconnections are bound pairs; i.e., disconnections exist as dipoles bound together by elastic interactions. However, for $T > T_{KT}$ the disconnections are unbound; i.e., each disconnection is free to move independently - not bound to any other disconnection.

The GB roughness, as characterized by the standard deviation of the GB profile σ_y scales as $\langle r^2/L^2 \rangle^{1/4}$ and diverges at T_{KT} (in 1D GB T_{KT} is also the roughening transition temperature). This is discussed in more detail in SI Appendix, demonstrated in our kMC simulations (below), and observed in MD simulations (16).

The mean-field theory reveals that the long-range elastic interaction between disconnections may result in the disconnection binding-unbinding (or pairing-unpairing) transition. However, mean-field analysis rarely provides accurate predictions of the phenomenon near a phase transition (and thus fails to predict T_{KT} accurately). This problem can often be overcome by application of renormalization group methods. Following the spirit of renormalization group approaches for dislocations (8, 17), we look for numerical solutions of Eq. (5) to obtain $f(l)$ and $g(l)$.

Any set of physical parameters/driving forces (K , b , h , E_c , T , ψ and τ) correspond to different initial conditions ($g(0), f(0)$) in the solution of Eq. (5); starting from each particular initial condition there is a flow in $(g(l), f(l))$ as l varies from 0 to ∞ (since l is a length scale, this is coarse-graining that takes the system to the thermodynamic limit). This is depicted in Fig. 2 for different $(g(0), f(0))$. Figure 2 shows that there are two types of fixed points as $l \rightarrow \infty$: (i) a “superfluid phase” ($g = 0, f \rightarrow \infty$), where screening diminishes dislocation interactions (i.e., $\epsilon \rightarrow \infty$) such that there are many unbound disconnection (i.e., $r^3 n \rightarrow \infty$) and the GB is rough, and (ii) an “insulating phase” ($g > 1.5, f = 0$), where screening is limited ($\epsilon < 2Kb^2 w / 3k_B T$ as $r \rightarrow \infty$), few unbound disconnections exist ($r^3 n \rightarrow 0$) and the GB is flat. There is a critical manifold (red curve) in Fig. 2; flows above the critical manifold converge to type (i) fixed points (unbound disconnection/rough GB phase), while flows below this manifold converge to type (ii) fixed points (bound disconnection/flat GB phase).

The KT transition temperature can be determined numerically. For a particular GB, $(g(l = 0, T), f(l = 0, T))$ is a parametric curve; temperature T is the parameter (the blue curve in Fig. 2). The point where the red and blue curves cross (Fig. 2) corresponds to T_{KT} . Formally, this temperature can also be determined from the condition that f is scale-invariant:

$$T_{KT} = [2Kb^2 \epsilon^{-1}(r_c) - (\psi h + \tau b) r_c] w / 3k_B, \quad [10]$$

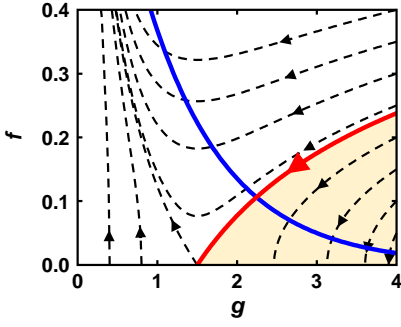


Fig. 2. Renormalization flows obtained by numerical solution of Eq. (5) with $\psi = \tau = 0$ and different initial conditions $(g(0), f(0))$. The arrows denote directions of increasing length scale l (coarse-graining). The red curve is the critical manifold. The flows in the shaded region converge to $(g > 1.5, f = 0)$ as $l \rightarrow \infty$, while the flows in the unshaded region converge to $(g = 0, f \rightarrow \infty)$. The blue curve corresponds to $(g(0, T), f(0, T))$ where the temperature T increases from bottom right to top left; the material and GB parameters are those used for the one-mode kMC simulation. The Kosterlitz-Thouless transition temperature corresponds to the point where the red and blue curves cross.

where r_c is the average disconnection separation in the dipoles at T_{KT} ($\epsilon(r_c)$ must be determined numerically). Eq. (10) is consistent with the mean-field result Eq. (9) ($\epsilon(r_c) = 1$) in the sparse disconnection ($E_c \gg Kb^2w$) and small driving force limits. When multiple disconnection modes are present, T_{KT} is dominated by the disconnection mode with the smallest T_{KT} .

Since the KT transition is associated with the screening of the long-range elastic interactions between disconnections and since disconnection motion is the underlying mechanism of GB migration, the KT transition should lead to a discontinuity in the temperature dependence of the GB mobility. When $T < T_{KT}$, the activation energy for GB migration Q includes both the disconnection glide barrier E^* and the large scale barrier associated with elastic interactions (9, 14, 18, 19); when $T > T_{KT}$, the elastic barrier is effectively screened. Hence, increasing T through T_{KT} leads to an abrupt decrease in the activation energy for GB migration Q ; the slope of the GB mobility versus temperature curve should increase abruptly upon heating through T_{KT} . Such an abrupt increase in the GB mobility slope versus T is observed at T_{KT} in the kMC simulations shown below.

Similar results were observed in the molecular dynamics (MD) simulations. Homer et al. (20) observed that the slope of the mobility versus temperature of the Ni $\Sigma 39$ [111] (752) symmetrical tilt GB changed abruptly at a finite T . For this GB, $b = a_0/\sqrt{26}$ and $h = 3a_0/\sqrt{78}$ (a_0 is the lattice constant)(9). With this input and the GB energy $\gamma \approx 0.5 \text{ J/m}^2$, thickness $w = 7.5a_0$, $K = 9 \text{ GPa}$ (assuming $r_c \sim w/2$ is the largest disconnection distance in this periodic cell), we find that $\epsilon = 7.6$ from Fig. 2. and (Eq. (10)) $T_{KT} \approx 800 \text{ K}$. So, the theoretical prediction of the temperature where an abrupt change of the activation energy for GB mobility is about 800 K, which is close to the MD result under $\psi = 0.025 \text{ eV}$. (20) The MD results of Homer et al. (20) also showed that the activation energy for GB migration Q is an approximately linear function of the “roughening temperature”, T_{KT} . We(19) previously showed that the activation energy for GB migration Q varies linearly with Kb^2 and Eq. (10) shows that Kb^2 is proportional to T_{KT} ; hence, Q is a linear function

of T_{KT} as observed in MD. Based on their MD simulations, Olmsted et al. (16) observed that at low temperatures and small driving forces, GBs migrate in a start-stop fashion, while at high temperatures/large driving forces, GBs migrate continuously. This may be understood by noting that below the KT transition ($T < T_{KT}$, which is driving force dependent), disconnection nucleation barriers are high thus disconnection nucleation time is much longer than migration time, while above the transition, nucleation (barriers) times are relatively short (disconnection screening effect) and are comparable with/smaller than migration times(19).

Kinetic Monte Carlo Simulations

Here, we compare the theoretical analysis with the results of disconnection-based kinetic Monte Carlo (kMC) simulations. Figure 1b shows the basic model employed in our kinetic Monte Carlo (kMC) simulations (the GB tilt axis and nominal GB normal are in z and y and the system is periodic in x). The GB is discretized into N lattice sites along x . The state of GB site i ($1 \leq i \leq N$) is denoted by $(u_i(t), y_i(t))$, where u_i is the relative (tangential) displacement of the upper grain with respect to the lower one (in x) and y_i is the position (in y) of the GB at site i . Formation of a pair of disconnections of mode m ($\pm b_m, \pm h_m$) at i corresponds to $(u_i, y_i) \rightarrow (u_i + b_m, y_i + h_m)$, as illustrated in Fig. 1b. See *Methods* for a detailed description of the kMC algorithm and the definition of the dimensionless quantities in this section. We report kMC results for two simulation cases: (i) a pure step mode, $h = 1$ and (ii) a single disconnection mode, $b = 1$ and $h = 1$.

For the parameters used in the kMC simulations, the renormalization group analysis (Fig. 2) predicts $T_{KT} = 0.1$ for the single disconnection mode kMC and $T_{KT} = 0$ for the pure-step simulations. The roughening transition ($\sigma_y \rightarrow \infty$ and spatial correlation length $\rightarrow \infty$) and screening/sliding transition ($\epsilon \rightarrow \infty$) occur at the same temperature T_{KT} for the case of a GB in a 2d bicrystal.

Figures 3a,b show the standard deviations of the GB profile $\sigma_y = \sqrt{\langle y^2 \rangle - \langle y \rangle^2}$, obtained from the kMC simulations. We recall that the roughening transition occurs at $T = 0$ for pure steps in 2d; this is consistent with Fig. 3a for which the roughness varies smoothly with temperature across the entire simulation temperature range. On the other hand, introduction of a finite disconnection \mathbf{b} (see Fig. 3b) effectively suppresses roughening at low T ($\lesssim T_{KT}$). At low T the roughness is nearly size-independent; this suggests the presence of very short-range correlations in the GB profile at low T . (The spatial correlation length ξ is the length scale over which the two-point correlation between the heights of different points on the surface decays with their separation.) Above T_{KT} , σ_y increases rapidly with T and a strong size effect (larger roughening in larger systems) is observed. The presence of the near linear dependence of roughness on temperature and a strong size dependence above T_{KT} is reminiscent of the roughening behavior in the pure step case (Fig. 3a) at $T > 0$. These are signatures of a finite- T transition.

In finite- \mathbf{b} systems, the standard deviation of the shear $\sigma_u = \sqrt{\langle u^2 \rangle - \langle u \rangle^2}$ (see the insets in Figs. 3b) show similar behavior as the GB profile roughening. The abrupt change in “shear roughening” suggests that shear roughening is also a characteristic of the disconnection KT transition T_{KT} . (In 3d, the GB profile and shear roughening need not occur at the

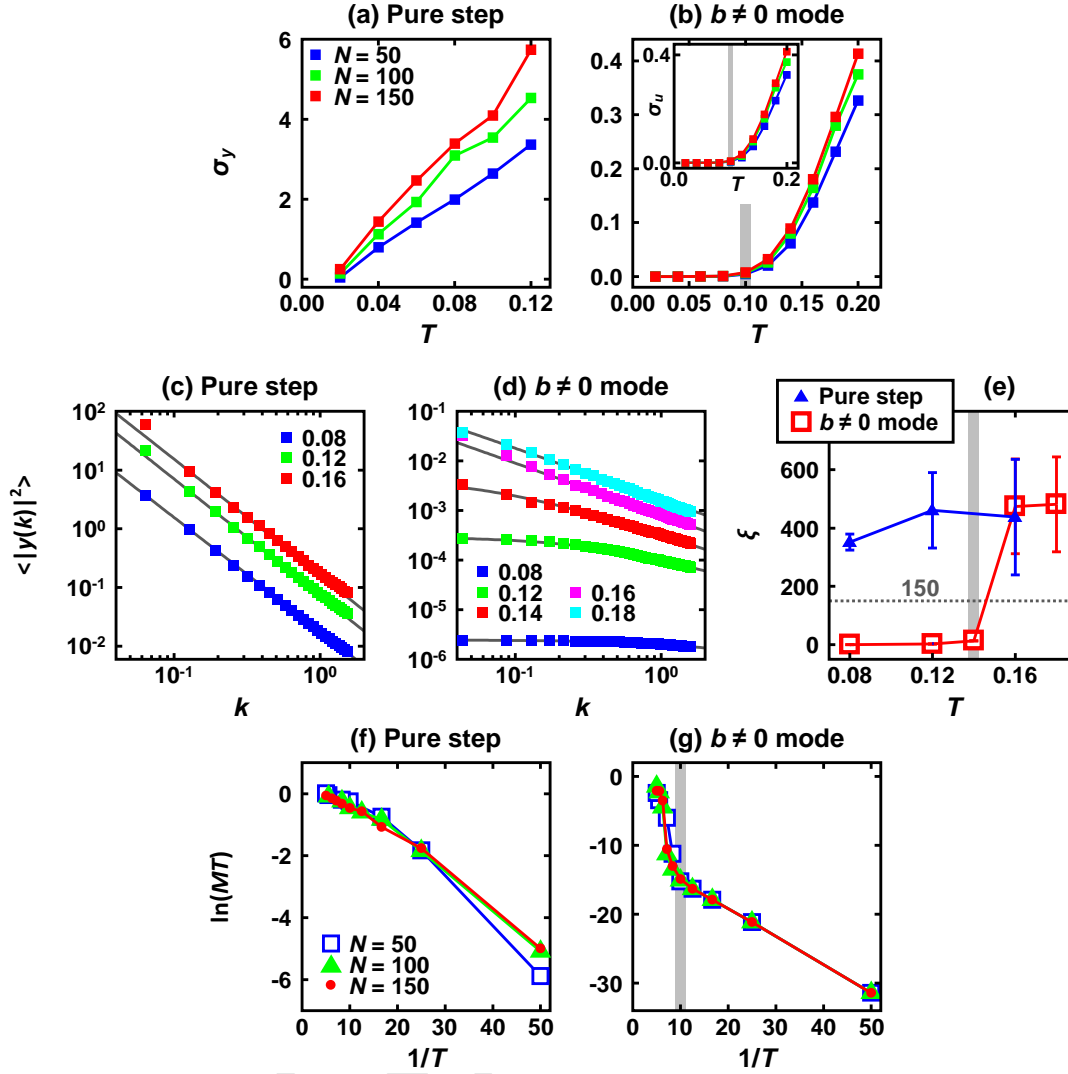


Fig. 3. (a)-(b) show the GB roughness σ_y vs. T for the (a) pure step and (b) single mode with $b \neq 0$; the insets in (b) is the standard deviations of shear σ_u vs. temperature T . (c)-(d) show the average of the (square of the) magnitude of the Fourier transform (k is a wave vector) of the equilibrium GB profile $y(x)$, $\langle |y(k)|^2 \rangle$, for several temperatures (see the legend) for the (c) pure step and (d) single mode with $b \neq 0$. (e) shows the correlation length $\xi(T)$ (obtained from fitting $\xi = AT/(k^d + \xi^{-d})$ for each temperature to the kMC data in (c)-(d); the horizontal dashed line (at $\xi = 150$) is the kMC simulation cell period (in x)). (f)-(g) show $\ln(MT)$ vs. $1/T$ (18), where M is the GB mobility for the (f) pure step and (g) single mode cases. The vertical gray lines label $T = 0.1$ in (b), and (g), and $T = 0.14$ in (e).

same T .)

Equilibrium fluctuations in the GB profile provide direct evidence of the GB roughening transition. We expand the GB profile in a Fourier series, $y(x, t) = \sum_k y(k, t)e^{ikx}$ and measure the equilibrium static GB profile spectrum $\langle |y(k)|^2 \rangle$, where $\langle \cdot \rangle$ represents a time average. Liao et al. (21) demonstrated that for pure steps, this spectrum should be described by

$$\langle |y(k)|^2 \rangle = T/[N\Gamma(k^2 + \xi^{-2})], \quad (11)$$

where ξ is the correlation length and Γ is the dimensionless GB stiffness. For disconnection with non-zero \mathbf{b} (22),

$$\langle |y(k)|^2 \rangle = T/[N\mathcal{B}^2(k^1 + \xi^{-1})], \quad (12)$$

where $\mathcal{B} \equiv b/h$ is the shear coupling factor. A correlation length ξ is introduced here as a wavelength cutoff (21). The KT transition theory suggests that $\xi \rightarrow \infty$ for $T > T_{KT}$ (21).

Figures 3c-d show the spectra obtained from the kMC simulations. These results indeed demonstrate that $\langle |y(k)|^2 \rangle \propto$

T , consistent with Eq. (11) and Eq. (12). The kMC data for each temperature were fitted to the function $AT/(k^d + \xi^{-d})$, where A , d and the correlation length ξ are the fitting parameters (d and ξ are functions of T). For $b = 0$ (Fig. 3c), $d \approx 2$, while when $b \neq 0$ (Figs. 3d), $d \approx 1$; consistent with Eqs. 11 and 12. The correlation length ξ obtained by the fitting at each temperature is shown in Fig. 3e. Since our kMC simulation were performed using a finite width GB ($N = 150$), we consider the GB roughened when $\xi > 150$. (Since ξ diverges above T_{KT} , it is not possible to obtain accurate measurements of ξ above T_{KT} .) Using this operational definition, we find that when $b = 0$ the GB is rough at all temperatures, but only rough at $T \geq 0.14 \approx T_{KT}$ for $b \neq 0$. The small difference between the theoretical prediction ($T_{KT} = 0.1$) and the simulation result ($T_{KT} = 0.14$) may be attributable to the finite GB width in the simulations and approximations in Eq. (11) and Eq. (12).

The GB mobility may be related(23) to fluctuations in the mean GB position \bar{y} : $M = N\bar{y}^2(\Delta t)/2\Delta tT$, where Δt is the

time interval used in the calculation of the time correlation \bar{y} . Figures 3f, g show the GB mobilities versus temperature from the kMC simulations. When the operative disconnection mode is a pure step mode (Fig. 3f), the GB mobility behaves in a quasi-Arrhenius fashion; $\ln(MT) \propto -Q/T$ (18), where the activation energy Q (i.e., slope of $\ln(MT)$ vs. $1/T$) is roughly temperature-independent (note that Q may exhibit a weak temperature dependence in cases where the disconnection nucleation and migration times are comparable (19)). When $b \neq 0$ (Fig. 3g), the activation energy Q (slope) changes abruptly at $T \approx T_{KT}$. This is because at $T > T_{KT}$, the disconnection elastic fields are effectively screened such that the elastic contribution to the activation energy for disconnection formation is zero. The temperature at which the activation energy for mobility changes ($b \neq 0$) coincides with an abrupt change in both σ_y and/or σ_u (Fig. 3b), i.e., T_{KT} .

The kMC simulations demonstrate that, when the activated disconnection mode has non-zero \mathbf{b} , a finite temperature dynamic phase transition occurs in the GB (provided melting does not occur first). Examination of the standard deviations of the GB profile σ_y and the equilibrium GB fluctuation spectrum $\langle |y(k)|^2 \rangle$ suggests that such a phase transition corresponds to the GB roughening transition. The simultaneous transitions in the behavior of the standard deviations of the GB shear σ_x , the divergence of correlation length ξ above critical temperature and the temperature dependence of GB mobility suggest that the roughening transition is a Kosterlitz-Thouless, topological phase transition. The kMC simulation results suggest that the abrupt changes in the temperature dependencies of σ_y , σ_x , $\langle |y(k)|^2 \rangle$ and M provides clear evidence of a transition temperature for GB dynamics with $b \neq 0$ disconnections (see Fig. 3) at a temperature consistent with the KT transition temperature T_{KT} predicted by the renormalization group theory, $T = 0.1$ (section *Disconnection Topological Transitions*). In other words, finite b disconnection-mediated KT transitions can result in both GB roughening and changes in GB migration behavior.

Grain Growth Stagnation

Grain growth stagnation is widely observed in both experiments (24) and MD simulations (1). Holm and Foiles suggested that this stagnation is associated with the GB roughening transition (1). Here, we argue that this behavior is better described in terms of the GB KT transition.

The driving force for grain growth is the reduction of the energy of the GB network in a polycrystal. In classical analyses of normal grain growth, we assume the GB energy is isotropic and GB migration is overdamped. This means that the GB velocity is proportional to its mean curvature H (i.e., mean curvature flow). The chemical potential jump across the GB is $\psi = \gamma H$ and the mean curvature scales (on average) as the inverse of the grain size, D ; ψ decreases as D increases. Eq. (10) shows that decreasing ψ (increasing grain size D) implies an increasing KT transition temperature, $T_{KT}(D)$. Therefore, during isothermal grain growth, the increase in the mean grain size results in fewer and fewer mobile grains (i.e., those with $T_{KT}(D) < T$). This may lead to grain growth stagnation.

The inverse of the critical grain size is

$$D_{KT}^{-1} = \left(\frac{1}{\epsilon(r_c)} - \frac{3k_B T}{2Kb^2 w} \right) \frac{Kb^2}{r_c \gamma h}. \quad [13]$$

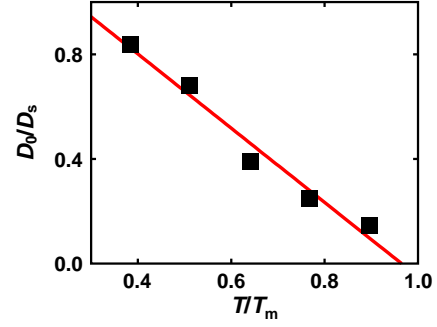


Fig. 4. Temperature dependence of stagnated grain size D_s from mesoscale MC simulations (data points) from Ref. (1) and a linear fit from Eq. (13). D_0 and T_m are the initial grain size and melting point, respectively.

Holm and Foiles observed grain growth stagnation at different temperatures in Monte Carlo simulations of polycrystals (1); their data (points in Fig. 4) shows that inverse mean grain size at which stagnation occurs D_s^{-1} varies with temperature T in an approximately linear function of T ; as predicted here, Eq. (13). When the grain size exceeds D_{KT} , the grain will stop growing or shrinking. Eq. (13) suggests that, grain growth continues when $T \geq 2Kb^2 w / 3\epsilon k_B \equiv T_c$ ($D_{KT} \rightarrow \infty$).

For nickel (assuming b , h , w and r_c are of the order of one lattice constant, $\epsilon \approx 1$, and $\gamma \approx 1$ J/m²), we find that $T_c \sim 18000$ K, which is much higher than the melting point. This implies that grain growth in polycrystalline nickel should always stagnate at a finite grain size, as observed in MD simulations (1). T_c may decrease substantially upon application of an external stress.

Since D_{KT} varies grain-to-grain in a polycrystal, some GBs will show very small mobilities while others will remain mobile. As noted by Holm et al. (25), this suggests that abnormal grain growth may readily occur prior to overall grain growth stagnation.

The GB mobility is a tensor, linking both GB shear coupling and migration (18). While the GB migration mobility shows a rapid increase at T_{KT} , the GB sliding coefficient will also increase rapidly at the KT transition temperature. This suggests the existence of a GB sliding transition; consistent with the widespread observations of the onset of superplasticity at small grain sizes or high temperature (2) and intergranular fracture at large grain size and low temperature in many materials (26).

Discussion

The theoretical analysis presented above demonstrates that GBs undergo a finite-temperature, Kosterlitz-Thouless, topological phase transition. The topological phase transition implies a transition from smooth to rough GBs, a transition from nearly immobile to highly mobile GBs, and a transition from non-sliding to readily sliding GBs. Because disconnections have dislocation, in addition to step, characters, this transition is topological in nature. While the step character is associated with the rapid change in GB mobility and GB roughening, the dislocation character is associated with the onset of GB sliding at T_{KT} .

The nature of the dynamic phase transition at GBs depends on disconnection character $\{\mathbf{b}, h\}$ and dimensionality (2d or 3d), as summarized in Table 1. For a pure step ($\mathbf{b} = 0$), the

Table 1. Transition temperatures for thermodynamic GB roughening and sliding and where abrupt changes in GB mobilities are expected for pure step ($\mathbf{b} = 0$), pure dislocation ($h = 0$), a single disconnection mode (\mathbf{b}, h), and multiple disconnection modes (\mathbf{b}_m, h_m). A “-” and “0” indicate no transition and a transition temperature at 0 K. The subscripts and superscripts indicate dimensionality (2d/3d) and pure step (S), pure dislocation (D), single disconnection (1), and multiple disconnection (M) modes. M_{11} , M_{12} and M_{22} represent mobilities associated with pure GB migration, shear coupling, and sliding, respectively(18). For multiple disconnection modes, entries only represent the lowest temperature of abrupt mobility changes.

| | Pure Step | | Pure Dislocation | | 1 Disconnection Mode | | Multiple Disconnection Modes | |
|------------|-----------|---------|------------------|---------|----------------------|---------|------------------------------|----------------------------|
| | 2d | 3d | 2d | 3d | 2d | 3d | 2d | 3d |
| Roughening | 0 | T_3^S | - | - | T_2^1 | T_3^1 | 0 | T_{3r}^M |
| Sliding | - | - | T_2^D | T_3^D | T_2^1 | T_3^1 | T_2^M | T_{3s}^M |
| Mobility | M_{11} | T_3^S | - | - | T_2^1 | T_3^1 | T_2^M | $\min(T_{3r}^M, T_{3s}^M)$ |
| | M_{12} | - | - | - | T_2^1 | T_3^1 | T_2^M | T_{3s}^M |
| | M_{22} | - | T_2^D | T_3^D | T_2^1 | T_3^1 | T_2^M | T_{3s}^M |

transition occurs at $T = 0$ in 2d and at finite T in 3d (15). Since this disconnection has $\mathbf{b} = 0$, such a transition leads to roughening and an increase in the GB migration mobility, but not to sliding. For a pure dislocation ($h = 0$), the transition occurs at finite temperature in both 2d and 3d. Since this disconnection has no associated step, such a transition leads to GB sliding, but not roughening. For GB dynamics with a single disconnection mode (finite \mathbf{b} and h), the phase transition leads to roughening, sliding, and a change in all types of mobilities at the same finite temperature $T = T_{KT} = T_d^1$.

While we do not explicitly consider multiple disconnection modes here, we expect that (i) the GB roughening will occur at $T = 0$ in 2d and at finite temperature (T_{3r}^M) in 3d (since pure step modes are always possible) and (ii) a sliding transition at finite temperature in both 2d (T_{2s}^M) and 3d (T_{3s}^M). In the multi-mode case, the mobilities will change abruptly at the topological transitions associated with both the thermodynamic roughening and sliding transitions. In 2d, the GB sliding transition temperature is associated with the smallest, nonzero Burgers vector. Above this temperature, all elastic interactions are screened ($\epsilon \rightarrow \infty$) and no additional KT transitions will occur; i.e., there is only one sliding transition in 2d (even when multiple disconnection modes are active). In 3d, two sliding transitions are possible since not all \mathbf{b} are parallel (i.e., the GB is two-dimensional).

Several researchers have demonstrated that grain growth in pure materials often stagnates at a finite grain size (1); stagnation is also seen as a pre-requisite to abnormal grain growth (a small set of grains grow to be much larger than the mean grain size) (25). Both stagnation and abnormal grain growth may further or hinder achievement of targeted material properties. The presented observations suggest that grain growth stagnation is associated with the difficulty of disconnection formation/migration below the GB transition temperature ($T < T_{KT}$; see Eq. 13 and Fig. 3). This is clear in our 2d simulations, where the GB mobility increases rapidly above T_{KT} (Fig. 3g) whereas the roughening temperature is 0 K (cf. Fig. 3a; the 2d multi-mode cases in Table 1).

Ample evidences (experiments, simulations and theories) demonstrate that many aspects of GB dynamics are associated with the formation and motion of disconnections (9). We presented mean-field and renormalization group theory results and kinetic Monte Carlo evidence for a finite-temperature, disconnection unbinding phase transition (of the Kosterlitz-Thouless type) in GBs. This disconnection unbinding phase transition is characterized by a finite-temperature transition in GB migration, roughening and sliding. Associated with

these are abrupt changes in the activation energies for the mobilities associated with GB migration and GB sliding at T_{KT} . These results provided a unified view of widely-observed feature of grain growth stagnation, abnormal grain, and superplasticity. Finally, we note that while other types of GB phase transitions (e.g., first-order structural phase transitions or other transitions in the atomic-scale structure of the GB) may occur and affect GB properties, the disconnection-based KT transition theory gives a unified vision of a wide range of physical phenomena and testable predictions of how these depend on both temperature and grain size.

Methods

The model adopted for the kMC simulations is shown schematically in Fig. 1b. The kMC algorithm is as follows.

- (i) Initialize the GB configuration (u_i, y_i) at each site i .
- (ii) List all possible events. The event (im) represents the nucleation of a disconnection pair of mode m at site i : $(u_i, y_i) \rightarrow (u_i + b_m, y_i + h_m) \equiv (u_i^+, y_i^+)$.
- (iii) Calculate the energy barriers for event (im) :

$$\Delta E_{im} = (\Delta E_{im}^c + W_{im}^I + W_m^E)/2 + E_m^*,$$

where ΔE_{im}^c is the change in core energy, W_{im}^I is the work done by the stress τ_i , W_m^E is the external work done by the driving forces, and E_m^* is the disconnection glide barrier. See Ref. (19) for the formula of each term.

- (iv) The rate associated with event (im) is $\lambda_{im} = \omega \exp(-\beta \Delta E_{im})$, where ω is the attempt frequency. The “activity” of the system is $\Lambda = \sum_{i,m} \lambda_{im}$.
- (v) Randomly choose an event with probability $p_{im} = \lambda_{im}/\Lambda$. Suppose that the selected event is $(i'm')$.
- (vi) Advance the clock by $\Delta t = \Lambda^{-1} \ln(\eta^{-1})$, where $\eta \in (0, 1]$ is a random number.
- (vii) Update the state at site i' as $u_{i'} := u_{i'} + b_{m'}$, $y_{i'} := y_{i'} + h_{m'}$ and the stress at each site. Return to Step (iii).

In the simulations shown, we set $\zeta = 0$, $\gamma = 0.1$, $E^* = 0.1\gamma(|b| + |h|)$. For the simulation of a GB in thermal equilibrium, we equilibrate the GB at each temperature in the absence of a driving force. All data is contained in the main text.

For simplicity, we employ the dimensionless variables: $\tilde{\gamma} = \gamma/2\pi K\delta$, $\tilde{h} = h/\delta$, $\tilde{b} = b/\delta$, $\tilde{y} = y/\delta$, $\tilde{t} = t\omega$, $\tilde{M} = 2\pi KM/\omega\delta$,

$\tilde{T} = k_B T / 2\pi K \delta^2 w$, $\tilde{\psi} = \psi / 2\pi K$, and $\tilde{\tau} = \tau / 2\pi K$. We drop the “tilde” in *Kinetic Monte Carlo Simulations* for notational simplicity.

ACKNOWLEDGMENTS. The research contribution of K.C., J.H., and D.J.S. (in part) was sponsored by the Army Research Office and was accomplished under Grant Number W911NF-19-1-0263. The views and conclusions contained in this document are those of the authors and should not be interpreted as representing the official policies, either expressed or implied, of the Army Research Office or the U.S. Government. The U.S. Government is authorized to reproduce and distribute reprints for Government purposes notwithstanding any copyright notation herein. D.J.S. also acknowledges support from the Hong Kong Research Grants Council General Research Fund 11211019. J.H. also acknowledges support from CityU Strategic Research Grant for unfunded GRF/ECS (SRG-Fd) 7005466, Hong Kong.

1. Elizabeth A. Holm and Stephen M. Foiles. How Grain Growth Stops: A Mechanism for Grain-Growth Stagnation in Pure Materials. *Science*, 328:1138–1141, 2010. . URL <https://www.jstor.org/stable/40656318>.
2. J. W. Edington, K. N. Melton, and C. P. Cutler. Superplasticity. *Progress in Materials Science*, 21(1-2):61–170, jan 1976. ISSN 00796425. .
3. Patrick R. Cantwell, Ming Tang, Shen J. Dillon, Jian Luo, Gregory S. Rohrer, and Martin P. Harmer. Grain boundary complexions. *Acta Materialia*, 62(1):1–48, jan 2014. ISSN 13596454. .
4. Timofey Frolov, David L. Olmsted, Mark Asta, and Yuri Mishin. Structural phase transformations in metallic grain boundaries. *Nature Communications*, 4(1):1–7, may 2013. ISSN 20411723. .
5. Thorsten Meinert, Timofey Frolov, Robert E. Rudd, Gerhard Dehm, and Christian H. Liebscher. Observations of grain-boundary phase transformations in an elemental metal. *Nature*, 579(7799):375–378, mar 2020. ISSN 14764687. . URL <https://www.nature.com/articles/s41586-020-2082-6>.
6. Craig Rottman. Roughening of low-angle grain boundaries. *Physical Review Letters*, 57(6):735–738, aug 1986. ISSN 00319007. . URL <https://journals.aps.org/prl/abstract/10.1103/PhysRevLett.57.735>.
7. Hao Zhang, David J. Srolovitz, Jack F. Douglas, and James A. Warren. Grain boundaries exhibit the dynamics of glass-forming liquids. *Proceedings of the National Academy of Sciences of the United States of America*, 106(19):7735–7740, may 2009. ISSN 00278424. .
8. J M Kosterlitz and D J Thouless. Ordering, metastability and phase transitions in two-dimensional systems. *J. Phys. C : Solid State Phys*, 6, 1973. URL [https://www.physics.uci.edu/~sim\\$taborek/publications/other/jcv6i7p1181.pdf](https://www.physics.uci.edu/~sim$taborek/publications/other/jcv6i7p1181.pdf).
9. Jian Han, Spencer L. Thomas, and David J. Srolovitz. Grain-boundary kinetics: A unified approach. *Progress in Materials Science*, 98:386–476, oct 2018. ISSN 00796425. . URL <https://www.sciencedirect.com/science/article/pii/S0079642518300641>.
10. William T.M. Irvine, Andrew D. Hollingsworth, David G. Grier, and Paul M. Chaikin. Dislocation reactions, grain boundaries, and irreversibility in two-dimensional lattices using topological tweezers. *Proceedings of the National Academy of Sciences of the United States of America*, 110(39):15544–15548, sep 2013. ISSN 00278424. . URL www.pnas.org/cgi/doi/10.1073/pnas.1300787110.
11. A P Sutton and R W Balluffi. *Interfaces in Crystalline Materials*. 1995. URL <https://pdfs.semanticscholar.org/55e5/8a63962445d2374728bf14808b560d27d8df.pdf>.
12. Koenraad G. F. Janssens, David Olmsted, Elizabeth A. Holm, Stephen M. Foiles, Steven J. Plimpton, and Peter M. Derlet. Computing the mobility of grain boundaries. *Nature Materials*, 5(2):124–127, feb 2006. ISSN 1476-1122. . URL <http://www.nature.com/articles/nmat1559>.
13. Spencer L. Thomas, Kongtao Chen, Jian Han, Prashant K. Purohit, and David J. Srolovitz. Reconciling grain growth and shear-coupled grain boundary migration. *Nature Communications*, 8(1):1–12, dec 2017. ISSN 20411723. . URL www.nature.com/naturecommunications.
14. Kongtao Chen, Jian Han, Spencer L. Thomas, and David J. Srolovitz. Grain boundary shear coupling is not a grain boundary property. *Acta Materialia*, 167:241–247, apr 2019. ISSN 13596454. .
15. Robert H. Swendsen. Roughening transition in the solid-on-solid model. *Physical Review B*, 15(2):689–692, jan 1977. ISSN 01631829. .
16. David L. Olmsted, Stephen M. Foiles, and Elizabeth A. Holm. Grain boundary interface roughening transition and its effect on grain boundary mobility for non-faceting boundaries. *Scripta Materialia*, 57(12):1161–1164, dec 2007. ISSN 13596462. . URL <https://www.sciencedirect.com.proxy.library.upenn.edu/science/article/pii/S1359646207005416>.
17. M Khantha, D P Pope, and V Vitek. Dislocation Screening and the Brittle-to-Ductile Transition: A Kosterlitz-Thouless Type Instability. *Physical Review Letters*, 1994. URL <https://journals.aps.org/prl/pdf/10.1103/PhysRevLett.73.684>.
18. Kongtao Chen, Jian Han, Xiaoqing Pan, and David J. Srolovitz. The grain boundary mobility tensor. *Proceedings of the National Academy of Sciences of the United States of America*, 117(9):4533–4538, mar 2020. ISSN 10916490. . URL <https://www.pnas.org/content/117/9/4533https://www.pnas.org/content/117/9/4533>.
19. Kongtao Chen, Jian Han, and David J. Srolovitz. On the Temperature Dependence of Grain Boundary Mobility. *Acta Materialia*, 194:412–421, aug 2020. ISSN 13596454. .
20. Eric R. Homer, Elizabeth A. Holm, Stephen M. Foiles, and David L. Olmsted. Trends in grain boundary mobility: Survey of motion mechanisms. *JOM*, 66(1):114–120, jan 2014. ISSN 10474838. . URL <http://link.springer.com/10.1007/s11837-013-0801-2>.
21. Maijia Liao, Xiao Xiao, Siu Tat Chui, and Yilong Han. Grain-Boundary Roughening in Colloidal Crystals. *Physical Review X*, 8(2), 2018. ISSN 21603308. . URL <https://journals.aps.org/prx/pdf/10.1103/PhysRevX.8.021045#page13>.

22. Alain Karma, Zachary T. Trautt, and Yuri Mishin. Relationship between Equilibrium Fluctuations and Shear-Coupled Motion of Grain Boundaries. *Physical Review Letters*, 109(9):095501, aug 2012. . URL <https://link.aps.org/doi/10.1103/PhysRevLett.109.095501>.
23. Zachary T. Trautt, Moneesh Upmanyu, and Alain Karma. Interface mobility from interface random walk. *Science*, 314(5799):632–635, oct 2006. ISSN 00368075. .
24. K. Barmak, J. Kim, C. S. Kim, W. E. Archibald, G. S. Rohrer, A. D. Rollett, D. Kinderlehrer, S. Ta’Asan, H. Zhang, and D. J. Srolovitz. Grain boundary energy and grain growth in Al films: Comparison of experiments and simulations. *Scripta Materialia*, 54(6):1059–1063, mar 2006. ISSN 13596462. .
25. E. A. Holm, M. A. Miodownik, and A. D. Rollett. On abnormal subgrain growth and the origin of recrystallization nuclei. *Acta Materialia*, 51(9):2701–2716, may 2003. ISSN 13596454. .
26. Norman E. Dowling. *Mechanical behavior of materials : engineering methods for deformation, fracture, and fatigue*. Pearson, 1999. ISBN 013905720X. URL [http://libnet.ac.il/\\$sim\\$libnet/pqd/opac_tau.pl?000421915](http://libnet.ac.il/simlibnet/pqd/opac_tau.pl?000421915).